Active Power Dynamic Interval Control Based on Operation Data Mining for Wind Farms to Improve Regulation Performance in AGC

Yushan Liu [1,2*], Lingmei Wang [1,2], Liming Chen[3], Enlong Meng [1,2], Huming Jia[4], Chengzhen Jia[1,2], Dongjie Guo[5], Shaoping Yin[1,2]

[1] School of Computer and Information Technology, Shanxi University, Taiyuan, People's Republic of China
[2] Wind Turbine Monitoring and Diagnosis NTRC of Shanxi Province, Taiyuan, People's Republic of China
[3] School of Computer, Ulster University, Belfast, UK
[4] Qinghai Green Power Operation and Maintenance Technology Co., LTD, Xining, People's Republic of China
[5] SPIC Shanxi New Energy Co., LTD, Taiyuan, People's Republic of China
*E-mail:18234004469@163.com

Abstract: With the real-time changes of wind speed and operating conditions, it is a challenge to fully tap the active power regulation ability and improve the control performance of automatic generation control (AGC) in a wind farm (WF). The essence of tapping the active power regulation ability is to realize the coordination and complementarity of each wind turbine's dynamic adjustment performance (DAP). To address this, a novel data mining method is developed to derive the internal relations between WTs' output power and pitch angle, impeller speed and pitch angle during the power adjustment process, and a unified mechanism model is established to describe DAP of wind turbines (WTs). Based on the discovered relationship between WTs' DAP and its operating states, an active power distribution algorithm and a dynamic interval control method (DICM) are proposed. Then, an active power dynamic interval control strategy that has been implemented using Java script in MyEclipse for WFs is further developed. The control strategy has been tested and applied in a 50MW WF in northwest China. The preliminary results showed that the control strategy has improved the rapidity and accuracy of AGC in the wind farm.

Nomenclature

AGC	automatic generation control
WF	wind farm
WT	wind turbine
DAP	dynamic adjustment performance
DICM	dynamic interval control method
PDA	proportional distribution algorithm
AWDA	ability weight distribution algorithm
MOOPA	multi-objective optimization algorithm
FICM	fixed interval control method
N-ICM	non-interval control method
TCOSP	trajectory curve of operating states point
PSPCS	power-speed-pitch angle curved surface
UAC	upward adjustment capacity
DAC	downward adjustment capacity
MAC	maximum adjustment capacity
UAR	upward adjustment rate
DAR	downward adjustment rate
ADZB	adjustment dead zone boundaries
UCIL	upper control interval limit
LCIL	lower control interval limit
CIB	control interval baseline
P_{pref}	AGC power commands
P_{output}	the output power of a WF
$\Delta Power$	a WF's output power adjustment amount
ΔP_i	the power adjustment amount undertaken by the i[th] WT
(v, β, ω, P)	a WT's operating states point
$f_1(\beta)$	the relationship between P changing with β
$g_1(\beta)$	the relationship between ω changing with β
v_{eig}	the wind speed characteristic value in the vertical direction of impeller
$\beta_{set-max}$	a WT's pitch angle protection limit
$\omega_{set-min}$	a WT's minimum impeller speed value
β_{max}	a WT's limit of pitch angle
ΔP_{up}	a WT's UAC
ΔP_{down}	a WT's DAC
ΔP_{max}	a WT's MAC
S_{power}^{up}	a WT's UAR
S_{power}^{down}	a WT's DAR
$(\tilde{v}, \tilde{\beta}, \tilde{\omega}, \tilde{P})$	N WTs' average operating states
$f_1^i(\beta)$	the i^{th} WT's $f_1(\beta)$
ΔP_{ADZB}	the adjustment dead zone range (ADZB)
P_{N-wf}	the installed capacity of a WF
$D_{ad}\%$	the scaling coefficient for the adjustment dead zone range.
$\Delta P_{control-region}$	the dynamic control region range
$D_{cr}\%$	the control region scale factor
$\Delta P_{safe-distance}$	the safety distance between the UCIL and the ADZB
$S_{output-power}$	the changing rate of a WF's output power
ΔT_{lag}	the response lag time of a WT
ΔT_{int}	the interval of data collection
ΔP_{inc}^t	the increment of P_{output} within ΔT_{int}
ΔP_i^{PDA}	the results of PDA
ΔP_i^{AWDA}	the results of AWDA
ΔP_i^{MOOPA}	the results of MOOPA
ΔP_i^{paper}	the results of the method in this paper
$S_{\Delta\beta}$	a WT's pitch angle adjustment rate

1. Introduction

According to the Global Wind Energy Council, the total global capacity of wind energy was over 651 GW in 2019, an increase of 10 percent compared with 2018, and the average growth rate of wind power capacity is expected to exceed 10% in the next five years [1]. The increasing penetration of wind power into the power systems around the world has led to various challenges due to the massive presence of non-synchronous generators in the power systems [2]. Among other problems, AGC is of great concern under the high wind penetration conditions, since additional wind installations will degrade the frequency response of power systems and increase the regulation requirement [3–4].

When the grid frequency drops, the inertia controller is a widely-used method specially to respond quickly to grid frequency drop during the first few seconds (less than ten seconds). It can be realized by designing proper inertia controllers or droop controllers to utilize the rotating kinetic energy of a wind turbine (WT) [5-6]. AGC is specifically used to respond to frequency drops within ten seconds to tens of seconds. This work only will study how to improve regulation performance in AGC for a WF.

Currently there are four ways to improve regulation performance in AGC for a WF. The first one is to utilize a separate energy storage device [7-10], however, the additional capital investment and maintenance cost of an energy storage system are too high, so the approach is unscalable and unsustainable. The second method is to integrate a novel adaptive controller into WTs' converters and main controller to improve the overall performance of wind energy conversion system [11-12]. The third method is to utilize both deloading and rotational kinetic energy control module to regulate grid frequency [13-15]. However, this method integrates the attuned-rotor speed control module into WTs' main controller. The control program for WTs needs to be modified, similar to the second method. The fourth method is to tap the potential of the WF's own active power regulation, which can improve the rapidity and accuracy of AGC without modifying the control program of the single WT and without additional cost. It is more economic and practical, and it has attracted a growing attention of many scholars in recent years.

The generic overview of the active power control strategy for a WF can be characterised and depicted in Fig. 1 (below the dotted line), where P_{AGC} denotes AGC power commands, P_{output} the output power of a WF, $\Delta Power$ is the output power adjustment amount of a WF, ΔP_i denotes the power adjustment amount undertaken by a WT. The essence of tapping the potential of the WF's own active power regulation is to improve the rapidity and accuracy of P_{output} in responding to P_{AGC} by distributing the $\Delta Power$ to each WT based on a certain algorithm and coordinating all WTs in real time. Different control strategies have different coordination control results. Some scholars formulated the coordination control problem as multi-objective optimization problems, which coordinate the power adjustment amount undertaken between WTs by multi-objective optimization algorithm (MOOPA) [16-22]. The minimum target power tracking error, the minimum energy consumption cost, and the minimum mechanical load of WTs are taken as the multi-objectives to optimize the output power of WTs, which is used to coordinate all WTs as a whole could optimally work at the desired operating states. However, this method considers that the adjustment performance of WTs, i.e. the output power adjustment rate of WTs are fixed, and the response time required to adjust the same power adjustment amount is the same. In fact, WTs' adjustment performance changes dynamically. Authors considered the dynamic characteristics of WTs' adjustment performance, and concluded that WTs' adjustment performance changes proportionally along with the output power. In their studies, a proportional distribution algorithm (PDA) distributed $\Delta Power$ to each WT and coordinated all WTs according to WTs' output power. In fact, under different wind speed, the adjustment performance of WTs with same output power varies greatly [23-25]. Some scholars [26-27] used wind speed to judge the change of a WT's operating states and measure the adjustment performance of the WT, and then coordinated all WTs according to the wind speed distribution difference between WTs. Nevertheless, even at the same wind speed, WTs with different pitch angle and impeller speed have large differences in their adjustment performance. As such, wind speed alone cannot accurately measure the adjustment performance, which will be further explained in the second section of this article. Authors took the pitch angle, rotation speed and wind speed of WTs as input, used fuzzy theory to evaluate the WTs' adjustment performance, and adopted the ability weight distribution algorithm (AWDA) to coordinate all WTs [28]. The control strategy of [16-28] is shown in Fig. 1 (below the dotted line). But the above control strategies have a few drawbacks. First, they do not have conducted a comprehensive system research on the law of the WTs' DAP changing with operating states, which causes WTs' power command mismatching its own adjustment performance and a long response time for WF to respond to AGC command. Second, they had not set the upper and lower limits of the interval around the target power. So, tracking the target value accurately in real time will bring frequent adjustment of WTs' power and increase the mechanical losses.

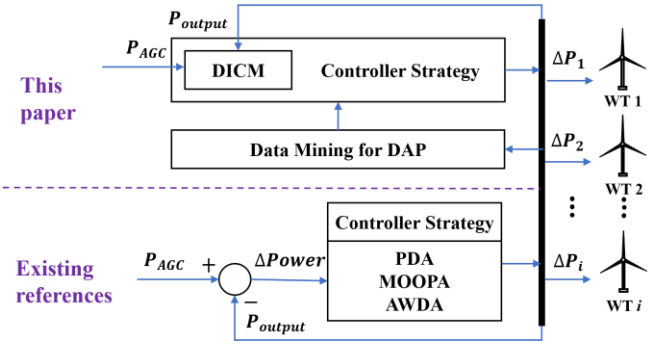

Fig. 1 *The control framework*

To solve above problems, a novel data mining method has been developed, which has sudied the law of the WTs' DAP changing with operating states, and an active power distribution algorithm based on WTs' DAP is proposed. Furthermore, a dynamic interval control method (DICM) to improve the accuracy of AGC of a WF has been developed. Then, an active power dynamic interval control strategy based on operation data mining for WFs is formed. The control framework of this paper is shown in Fig. 1 (above the dotted line). The real-time DAP among WTs are fully

coordinated and the synchronization of the output power regulation among WTs are achieved in this control strategy, then the output power of the WF is also adjusted to the fastest direction, and the active power regulation potential of the WF is maximized. Some scholars applied an optimised non-integer controller to the microgrid to improve regulation performance in AGC for the microgrid system [29-30]. In future research, the proposed control strategy will be applied to the microgrid. The contributions of this paper include:

(i) Put forward the concept of WTs' DAP and develop WTs' DAP research method that mines the trajectory curve of operating states point (TCOSP) from the actual input data (v), control data (β, ω) and output data (P), without making any simplified assumptions about WTs. The evaluating indexes for WTs' DAP are put forward, which are based on the TCOSP.

(ii) The proposed control strategy achieves consistency of the output power response time between the single WT and the entire WF. The differential distribution of active power adjustment amount between WTs are calculated according to the difference in the DAP of WTs under different operating states, which is based on the principle that a WT with larger output power adjustment rate undertakes more regulation tasks.

(iii) Develop a DICM for the proposed strategy. Compared with the fixed interval control method (FICM) and non-interval control method (N-ICM), the proposed method can improve the accuracy of the output power of a WF and reduce frequent adjustment of WTs.

The rest of this paper is organized as follows: Section 2 introduces a WT's DAP research method, and introduces how to mine the dynamic characteristics of WTs' DAP from actual operating data. Section 3 describes an active power distribution algorithm. Section 4 describes the control principle of DICM. Section 5 presents an active power dynamic interval control based on operation data mining for WFs, and elaborate control process and core frame of the control strategy in detail; Section 6 applies the control strategy to a WF and evaluates the control strategy through case studies, also, outlines the analysis results of actual application data. Section 7 concludes this paper.

2. Research on the DAP of WTs Based on Operation Data Mining

A WT's adjustment performance is closely related to its current operating states, including nacelle wind speed v, pitch angle β, impeller speed ω, output power P. WTs with different operating states have large differences in their adjustment performance, i.e. time-varying as the operating state changes. The DAP of a WT is difficult to be described by a unified mechanism model because it is closely related to the trajectory curve of operating states point (v, β, ω, P), which is different owing to different WT manufacturers, different models and different geographical locations. So, it is necessary to find this trajectory from actual operational data.

The conventional generator unit's adjustment performance refers to the adjustment rate and adjustment capacity changes with the operating state when it responds to the target power. Firstly, the TCOSP that is a prerequisite to research the DAP of WTs is mined. The nacelle wind speed v is measured by a mechanical anemometer placed behind the impeller on the top of the nacelle, there is measurement error, and it does not really reflect the real-time wind speed perpendicular to the impeller, so it cannot be directly used to analyse the DAP of WTs. It is necessary to find an effective wind speed that truly reflects the wind flowing through an impeller instead of the nacelle wind speed v. In this section, the mechanism of WTs' operating state changes during power regulation is analysed firstly. Then, the eigenvalues of the wind speed that flow through the impeller is extracted. Following this, the TCOSP is mined. Finally, the evaluating index of WTs' DAP and detailed calculation method are given.

2.1. The mechanism of WTs' operating state change

The mechanical power P_m of a WT can be expressed as [31]:

$$P_m = \frac{1}{2}\rho v^3 \pi R^2 C_p(\omega, \beta, v) \tag{1}$$

$$C_p(\omega, \beta, v) = 0.5176\left(\frac{116}{\lambda_i} - 0.4\beta - 5\right)e^{-\frac{12.5}{\lambda_i}} + 0.0068\lambda \tag{2}$$

$$\frac{1}{\lambda_i} = \frac{1}{\lambda + 0.08\beta} - \frac{0.035}{\beta^3 + 1} \tag{3}$$

$$\lambda = \frac{\omega R}{v} \tag{4}$$

Where: ρ is air density, v is the effective wind speed of the impeller, R is the radius of the impeller, ω is the impeller rotational speed (hereinafter referred to as the rotational speed), β is the pitch angle of the blade, $C_p(\omega, \beta, v)$ is the wind energy utilization coefficient, λ is the tip speed ratio. Under the Free-Generation Operation Mode (without receiving the target power command), a WT takes the maximum power tracking as its control target and makes maximum use of wind energy to generate electricity. The power curve is shown by the black solid line ABCD in Fig. 2.

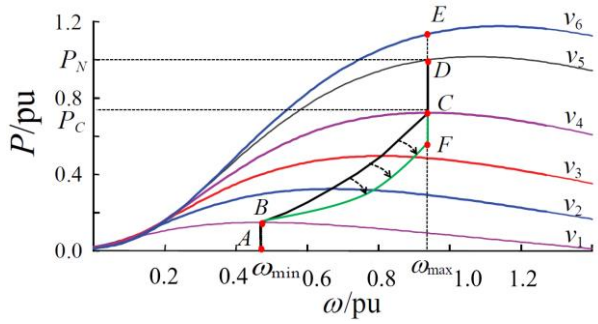

Fig. 2 *The power characteristic curve of a WT*

When a WT receives a target power command P_{set}, the wind energy absorbed by the WT is controlled through pitch adjustment and speed adjustment, so as to reduce the power output. This will lead to Power characteristic curve being transferred from ABCD to ABFC. The essence of power regulation is to find a proper C_{pset} through the

controlling of pitch angle β and rotational speed ω, so that the mechanical power obtained by a WT can be adjusted to the target value P_{set} deviating from the P_{opt} curve. The power curtailment control of WTs includes two ways: active pitch control, pitch and rotor speed coordinated control [32-34]. The first type of WTs adjusts the absorbed wind energy through its pitch angle control, which makes it deviate from P curve. In a certain wind speed, with the increase of pitch angle β, the mechanical torque decreases gradually, and the rotational speed ω is forced to pull down. Its TCOSP is shown in the green solid line OPMN (Trajectory projected to $P-\omega$ coordinate) in Fig. 3. Point O is the working point under the free power generation operation mode, $P_{m(max)}$ is the corresponding maximum output power, P and M are the steady-state operating points under the power setting values P_{set1} and P_{set2} respectively. The second type of WTs releases the absorbed mechanical energy through active speed control firstly without adjusting the pitch angle. If the WT's output power needs to be further reduced when its running status moves to point P_1 in Fig. 3, it needs to activate pitch control. Its TCOSP is shown in the black solid line $OP_1M_1N_1$ (Trajectory projected to $P-\omega$ coordinate) in Fig. 3. This paper only studies the first type of WTs.

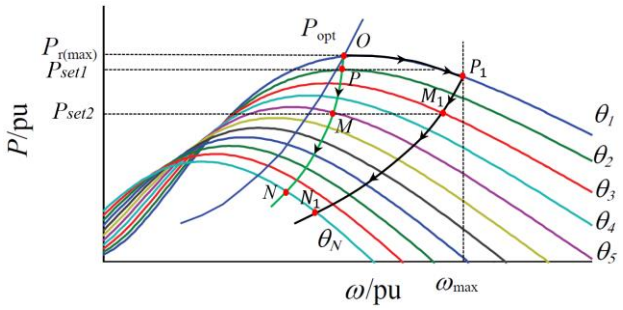

Fig. 3 *The TCOSP of a WT under fixed wind speed*

As can be seen in (1)-(4), under a certain wind speed, a WT's output power P is a binary function of ω and β. P , ω and β constitute a power-speed-pitch angle curved surface (PSPCS) as shown in Fig. 5, which is the PSPCS of the 2.0MW doubly-fed WT under different wind speeds in this paper. During the power regulation, the TCOSP is a spatial curve in the PSPCS. When the wind speed $v=v_0$, the equation of the TCOSP can be expressed by the following (5):

$$\begin{cases} P=f_1(\beta) \\ \omega=g_1(\beta) \end{cases} \tag{5}$$

2.2. Extraction of effective wind speed characteristic value in vertical direction of the impeller rotating plane

A WT adjusts the absorbed wind energy through its pitch and speed control. The track composed of a series of operating state points (v,β,ω,P) is a spatial curve (v is the nacelle wind speed) in the spatial surface PSPCS. As such, the wind speed characteristic value can truly reflect the absorbed wind energy. Under any initial operating state $(v_0,\beta_0,\omega_0,P_0)$, when β_0、ω_0、P_0 are introduced into (1)-(4), a complex nonlinear equation about wind speed v can be got shown in (6).

$$P_0=\frac{1}{2}\rho v^3\pi R^2C_p(\omega_0,\beta_0,v) \tag{6}$$

Given the range of solution $[v_0-\Delta v_c, v_0+\Delta v_c]$, let's set:

$$F(v)=P_0-\frac{1}{2}\rho v^3\pi R^2C_p(\omega_0,\beta_0,v) \tag{7}$$

In combination with (2)-(4), the dichotomy method is used to solve (7), and the solution v_{eig} is the wind speed characteristic value. The solution process is shown in Fig. 4. ε_1、ε_2 are infinitesimal positive numbers close to zero.

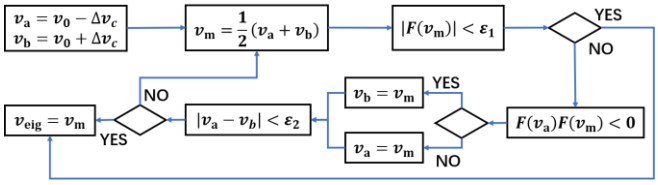

Fig. 4 *Flow chart of* $\boldsymbol{v_{eig}}$ *solution*

The unique spatial surface PSPCS can be determined when v_{eig} is given. In the spatial surface PSPCS, there is only one TCOSP. If there are more than one, the WT operation will be unstable, that is to say v_{eig} is one-to-one corresponding to the spatial surface PSPCS and the TCOSP. The v_{eig} is equal on the same curve. As shown in Fig. 5, the three points A_1, A_2 and A_3 under any operating state of WTs can determine their respective operation trajectory curves, and also determine the unique v_{eig}^1 、 v_{eig}^2 、 v_{eig}^3 corresponding to them. Therefore, when a WT is operating in any two different states, the effective wind speed in vertical direction of impeller rotating plane can be compared using the value of v_{eig}. That is to say v_{eig} can describe the effective wind speed value in any operating state. In this paper v_{eig} is called the wind speed characteristic value in the vertical direction of impeller rotating plane.

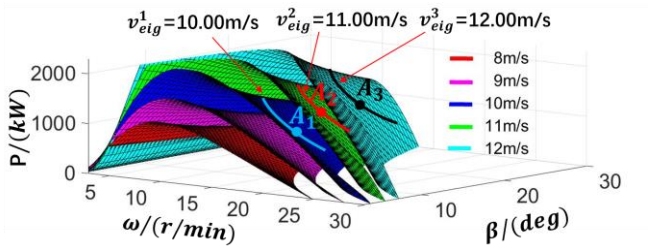

Fig. 5 *PSPCS spatial surface under different* $\boldsymbol{v_{eig}}$

2.3. Mining the TCOSP

WTs' second level operation SCADA data is used to deeply mine the TCOSP and fit the trajectory curve equation. It can be seen from the analysis in 2.2 that v_{eig} describes the effective wind speed value of an impeller under any operating state, and has an one-to-one correspondence to TCOSP. To analyse TCOSP, the v_{eig} is divided into n segments instead of the nacelle wind speed v, and fit the trajectory curve equation in segments. The basic steps are as follows:

(i) Data preparation: the data of time, nacelle wind speed v, pitch angle β, impeller speed ω, generator output power P are extracted from a large amount of SCADA

second-level data. In this process, the data collected during WT shutdown and disconnection of a WT are eliminated from the grid based on the output power P i.e., zero or less than zero. The remaining data is recorded as dataset A.

(ii) Dataset A pre-processing: the wind speed characteristic value v_{eig} corresponding to each second data is calculated by using the method in 2.2, and two significant figures are reserved for v_{eig}. v_{eig} is used to replace the nacelle wind speed v, and the replaced data is recorded as dataset B. After replacement, the operating state point of a WT will be expressed as $(v_{eig}, \beta, \omega, P)$.

(iii) Fitting of the TCOSP. Firstly, v_{eig} is divided into n segments from v_{cut-in} to $v_{cut-out}$ according to the accuracy of Δv_{dif}, then in data B, the data of each v_{eig} segment $\left[v_{eig}^{i} - \Delta v_{dif}, v_{eig}^{i} + \Delta v_{dif}\right]$ are extracted, then $P-\beta$ and $\omega-\beta$ scatter diagrams are generated respectively. It can be known from the above analysis that the monotonicity and convexity of $f_1(\beta)$ and $g_1(\beta)$ remain unchanged during the power adjustment process. Fig. S1 and Fig. S2 (see in Support Information) show the parameter fitting results of $f_1(\beta)$ and $g_1(\beta)$ when v_{eig} is 10.5 m/s. These discrete points are fitted with polynomials, and the goodness of fitting (R-square) is greater than 0.99, and the accuracy meets the fitting requirements.

Therefore, the relationship between P changing with β, and ω changing with β can be assumed as follows:

$$f_1(\beta) = a_1\beta^3 + b_1\beta^2 + c_1\beta + d_1 \quad (8)$$

$$g_1(\beta) = a_2\beta^3 + b_2\beta^2 + c_2\beta + d_2 \quad (9)$$

There are many methods for fitting curves, such as the best straight line fitting, neural network fitting, and least square polynomial curve fitting. From v_{cut-in} to $v_{cut-out}$, a curve fitting can be divided into n stages. Since there are many scattered points in each stage, and n stages need to be carried out automatically and continuously, the least square polynomial curve fitting method has the advantages of good stability, approximation, convenient and fast calculation, and easy implementation of the program. Therefore, the least square polynomial curve fitting method is selected to fit the discrete points in each segment.

2.4. The evaluation index of DAP

The response time, regulation capacity, regulation accuracy and failure rate can usually be selected as the evaluation indexes of adjustment performance for a conventional power plant. Based on the mechanism of WTs' operating state change, the regulation capacity and regulation rate are selected as the DAP evaluation indexes in this paper.

2.4.1 Adjustment capacity: In this paper, the adjustment capacity includes upward adjustment capacity (UAC), downward adjustment capacity (DAC) and maximum adjustment capacity (MAC). As shown in Fig. 6, P_{max} and P_{min} are the maximum and minimum output power that a WT can achieve respectively through active adjustment under the current operating state . The UAC and DAC are the corresponding difference between P_{max}, P_{min} and the current output power of a WT while the MAC is the difference between P_{max} and P_{min}.

P_{max} is referred to the maximum output power of the corresponding Free-Generation Operation Mode under the current working conditions, which can be calculated by (10):

$$P_{max} = \begin{cases} f_1(\beta_{min}), & f_1(\beta_{min}) \le P_N \\ P_N, & f_1(\beta_{min}) > P_N \end{cases} \quad (10)$$

Where β_{min} is the minimum pitch angle during operation below rated power, which is usually taken as zero, and P_N is the rated power of a WT. When a WT reduces power through active adjustment, the pitch angle increases and the impeller speed is pulled down passively. Without shutdown, the limit of pitch angle and speed that a WT can reach, i.e., the pitch angle protection limit $\beta_{set-max}$ and the minimum speed value $\omega_{set-min}$, will determine the minimum output power P_{min}, can be calculated by combining (8) and (9). Let:

$$g_1(\beta) = \omega_{set-min} \quad (11)$$

By solving the (11), the $\beta_{\omega min-max}$ can be got. It is the maximum pitch angle restricted by the minimum speed. In the process of power reduction, the limit of pitch angle that a WT can reach is:

$$\beta_{max} = min\{\beta_{set-max},\ \beta_{\omega min-max}\} \quad (12)$$

The minimum power value that a WT can achieve is:

$$P_{min} = f_1(\beta_{max}) \quad (13)$$

As shown in Fig. 6, under the given v_{eig}, when a WT is operating at point Q, the UAC ΔP_{up} can be calculated by (14):

$$\Delta P_{up} = P_{max} - P_Q \quad (14)$$

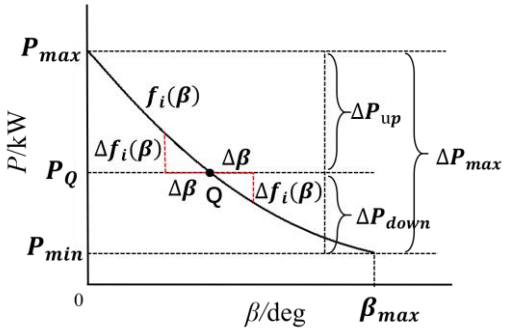

Fig. 6 *The calculation principle of DAP evaluation index*

The DAC ΔP_{down} can be calculated by (15):

$$\Delta P_{down} = P_Q - P_{min} \quad (15)$$

The MAC ΔP_{max} can be calculated by (16):

$$\Delta P_{max} = P_{max} - P_{min} \quad (16)$$

2.4.2 Adjustment rate: The regulation rate in this paper refers to the change rate of $f_1(\beta)$ at the operating point $\beta = \beta_0$, which reflects the sensitivity of output power to the change of the pitch angle in the process of power regulation. The adjustment rate includes upward adjustment rate (UAR)

and downward adjustment rate (DAR). As shown in Fig. 6, under the given v_{eig}, when a WT is operating at point Q, the UAR S_{power}^{up} can be calculated by (17):

$$S_{power}^{up} = \frac{\Delta f_1(\beta)}{\Delta\beta} = \frac{f_1(\beta - \Delta\beta) - P_Q}{\Delta\beta} \quad (17)$$

The DAR S_{power}^{down} can be calculated by (18):

$$S_{power}^{down} = \frac{\Delta f_1(\beta)}{\Delta\beta} = \frac{P_Q - f_1(\beta + \Delta\beta)}{\Delta\beta} \quad (18)$$

Where $\Delta\beta$ is the pitch angle adjustment amount. When $\Delta\beta$ is small enough, the UAR and DAR are equal.

2.5. The analysis of TCOSP and DAP

A WF in the Northwest China, has been used as the research and evaluation context for this study, which consists of 25 2MW doubly-fed induction generators. Table. S1 (see in Support Information) shows relevant details of the WTs in the WF. A total of more than 648 million sets of SCADA second-level operating data extracted from all WTs of the WF in March 2019 are analysed to test, evaluate and also demonstrate the proposed strategy. The configuration parameters of various analysis methods are written using Java script and displayed in Table. S4 (see in Support Information). The method in the section 2.3 is used to fit TCOSP. WTs with lower wind speed usually do not participate in the power regulation of the WF, so there are few limited power operation points in the interval of 3 m/s - 4.5 m/s. In this paper, the initial v_{eig} is 4.6 m/s, the maximum v_{eig} is 22 m/s, and the value of Δv_{dif} is 0.02, so there are 435 wind speed segments. The value of Δv_{dif} is 0.02, which is based on substantial engineering experience. If Δv_{dif} is too small, there will be few operating state points (v, β, ω, P) in each v_{eig} segment, and $f_1(\beta)$, $g_1(\beta)$ are difficult to reflect the TCOSP accurately. Meanwhile, if Δv_{dif} is too large, the $f_1(\beta)$ and $g_1(\beta)$ will be over-fitting. The fitting results of $f_1(\beta)$ and $g_1(\beta)$ are shown in Table. S2 (see in Support Information). Fig. S3 (see in Support Information) shows the TCOSP under different v_{eig}.

Fig. 7 (a) is the trajectory curve projected from the spatial curve in Fig. S3 to the $P-\beta$ coordinate. Under a certain v_{eig}, the output power gradually decreases with the increase of pitch angle. The minimum output power P_{min} that a WT can achieve is limited by $\beta_{set-max}$ and $\omega_{set-min}$ without shutdown. When v_{eig} is less than 9 m/s, P_{min} is limited by $\omega_{set-min}$, when v_{eig} is greater than 9 m/s, P_{min} is limited by $\beta_{set-max}$. Fig. 7 (b) shows the change curve of a WT's DAR with its pitch angle under different v_{eig} (the UAR is similar to it). Under the same v_{eig}, the DAR gradually decreases with the increase of pitch angle, i.e. the sensitivity of the output power to the changing of the pitch angle gradually decreases. By changing the same $\Delta\beta$, the amount of change in output power gradually decreases. Fig. 7 (c) and (d) respectively show the change curves of UAC and DAC with the pitch angle under different v_{eig}. It can be seen that the UAC increase with the pitch angle increasing, and the DAC decreases gradually. When the pitch angle increases to $\beta_{set-max}$, the UAC reaches the maximum value, and the DAC decreases to zero.

The DAP of a WT is changing dynamically in accordance with the position of its operating states point in the TCOSP curve. WTs operating in different states have different adjustment capacities and adjustment rates. Even when WTs executes the same active power adjustment command ΔP, their adjustment amount of pitch angle are different. Even when WTs under different operating states change the same pitch angle, their active power adjustment amount ΔP are also different. Therefore, there is a need for coordination and complementarity between the DAP of WTs.

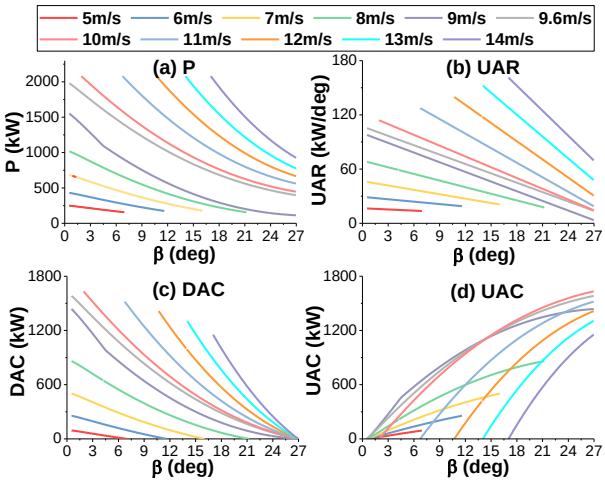

Fig. 7 *DAP curve*

In addition, the characteristic value v_{eig}, which corresponds to the TCOSP, can represent the effective value of the wind speed in the vertical direction of the impeller rotating plane. The calculation of v_{eig} is the premise of mining the TCOSP, which is the premise for studying the DAP. Therefore, the calculation method of v_{eig} is crucial.

3. Active power distribution algorithm

The adjustment rate and adjustment capacity of a WT change dynamically along with the changing of the WT's operating states. Since WTs in a WF are widely distributed, there is a large variance in the wind speed and operating states of each WT at any specific time point, leading to large differences in DAP of each WT. This section describes how to design an active power distribution algorithm for a WF which can fully coordinate the DAP of WTs in different operating states and reasonably distribute the power adjustment amount undertaken by each WT, thus improving the rapidity of AGC. Before distributing the power adjustment amount to each WT, it is necessary to determine the control sequence of the controlled WTs, i.e. to determine the combination of WTs participating in a WF's power regulation.

3.1. Control sequence determination of the controlled WTs

The basic idea of determining the control sequence of the controlled WTs is as follows: when a WF receives the power command of AGC requiring it to adjust the power, under the current operation states of WTs, it will select an appropriate number of WTs with excellent DAP to be

controlled, which can not only avoid unnecessary mechanical loss caused by too many WTs participating in the regulation, but also can achieve the rapid adjustment of the active power of the WF. Therefore, the determination of control sequence of the controlled WTs includes the label index of controlled WTs and WTs' numbers.

The number of controlled WTs is determined firstly. Assume the number of controllable WTs other than the template WTs (which do not participate in power regulation, and are used to calculate the loss of electricity due to wind curtailment) is N. If the WF has multiple types of WTs, data mining is required for each type of WTs according to steps (i)-(iii) in section 2.3 to fit the parameters of $f_{1\_X}(\beta)$ and $g_{1\_X}(\beta)$. X represents the type of WTs. $f_{1\_X}(\beta)$ is the $f_1(\beta)$ of the X type WTs. $g_{1\_X}(\beta)$ is the $g_1(\beta)$ of the X type WTs. The average operating state $(\widetilde{v_X}, \widetilde{\beta_X}, \widetilde{\omega_X}, \widetilde{P_X})$ is calculated for each type of WTs by calculating the average wind speed, average pitch angle, average rotational speed and average output power. The number of controlled WTs N_c, is determined as follows:

When a WF needs to increase power:

$$N_c = \begin{cases} \dfrac{\Delta Power}{\sum E_X\left(f_{1\_X}(\widetilde{\beta_X} - \Delta\beta_c) - \tilde{P}\right)}, & \widetilde{\beta_X} - \Delta\beta_c \geq 0 \\ & , f_{1\_X}(\widetilde{\beta_X} - \Delta\beta_c) < P_N^X \\ \dfrac{\Delta Power}{\sum E_X\left(P_N^X - \tilde{P}\right)} & , f_{1\_X}(\widetilde{\beta_X} - \Delta\beta_c) \geq P_N^X \end{cases} \tag{19}$$

When a WF needs to reduce power:

$$N_c = \begin{cases} \dfrac{\Delta Power}{\sum E_X\left(\tilde{P} - f_{1\_X}(\widetilde{\beta_X} + \Delta\beta_c)\right)}, & \widetilde{\beta_X} + \Delta\beta_c \leq \beta_{max}^X \\ \dfrac{\Delta Power}{\sum E_X\left(\tilde{P} - f_{1\_X}(\beta_{max}^X)\right)} & , \widetilde{\beta_X} + \Delta\beta_c \geq \beta_{max}^X \end{cases} \tag{20}$$

In the (19) and (20), $\Delta Power$ is the adjustment amount of the output power of a WF, E_X is the ratio of the sum of type X controlled WTs' capacity to the total controlled WTs' capacity, β_{max}^X is the β_{max} of type X WTs, P_N^X is the rated capacity of type X WTs, $\Delta\beta_c$ is the minimum adjustment amount of the pitch angle of the controlled WTs, and the calculation starts with 1. If N_c is less than N, N_c is the number of controlled WTs; Otherwise, $\Delta\beta_c$ is increased by 1. If $N_c$is greater than N, $\Delta\beta_c$ is increased by 1 until N_c is less than N. The final calculated N_c is the number of controlled WTs. The calculation of $\Delta\beta_c$ starts at 1 for two reasons. First, during the power regulation process, the pitch angle adjustment rate is 1-2 deg/s, i.e. it takes less than 1s to adjust the pitch angle by 1deg; Second, when a WT is operating at constant power state, the pitch angle will adjust frequently to adapt to the continuous fluctuation of wind speed, so that it can maintain the constant output power. In real situations the output power will fluctuate near the power command, usually the fluctuation range is ±1%. If the value of $\Delta\beta_c$ is too small, the number of controlled WTs will increase, and the output power value of each controlled WT will be too small to be recognized. If the value of $\Delta\beta_c$ is too large, the number of controlled WTs will be small, and the adjustment rate of a WF's output power will be slow. 1 is the engineering experience value, which is selected based on experience during a large number of debugging processes. In future research, a multi-objective optimization algorithm is used to calculate the optimal value of $\Delta\beta_c$.

Then, the indexes of the controlled WTs are determined. These N controllable WTs in a WF shall be sorted according to the adjustment rate. Using the (17) and (18), the UAR and DAR of these WTs at current operating state can be calculated. When the WF active power increasing is needed, the N controlled WTs should be sorted based on UAR. When it needs to reduce power, the controlled WTs should be sorted based on the DAR. After the ranking, take the first N_c WTs as the control sequence of controlled WTs.

3.2. Active power distribution algorithm

A WT controls the output power through active pitch control. When any two WTs under different operating states change the same pitch angle, their corresponding required times are same. When the time required to adjust the power of all controlled WTs are the same, the time required to adjust the output power of the entire WF will be the shortest. In order to coordinate and maximize the different DAP of WTs under different operating states, the active power distribution algorithm for a WF based on the following basic ideas is designed: a WT with a larger adjustment rate can undertake more active power adjustment amount, according to the same amount of pitch angle adjustment for selected WTs. It can further synchronise the power regulation of any individual WTs with that of the WF as a whole, thus making the output power response time of a single WT consistent with that of the entire WF. In this case, the active power adjustment rate of a WF is the fastest, therefore the response time is the shortest. The design principle of this algorithm is shown in Fig. 8. $f_1^i(\beta)$ is the trajectory curve of the TCOSP projected in P-β coordinates for ith WT at the current moment, i.e. the relationship between the output power P_i and the pitch angle β_i. $f_1^i(\beta)$ is changing dynamically with the change of the operating state $(v_i, \beta_i, \omega_i, P_i)$. Under different operating states, the sensitivity of a WT's output power to the change of the pitch angle is different, i.e. the adjustment rate is different. As shown in Fig. 8, when the pitch angle of all controlled WTs is adjusted by the same amount of change $\Delta\beta$:

$$\Delta\beta = n\Delta\beta_s \tag{21}$$

Where $\Delta\beta_s$ is the minimum adjustment amount of the pitch angle when calculating the active power distribution.

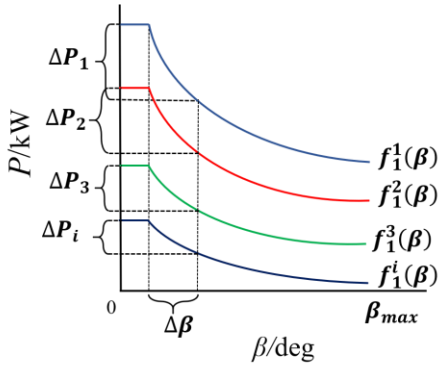

***Fig.** 8 The principle of active power distribution algorithm*

The adjustment amount ΔP_i of a WT's output power is calculated according to the curve $f_1^i(\beta)$, where n is the number of cycles. With the increase of n (β_i decreases when a WF increases its output power, and vice versus), when the sum $\sum \Delta P_i$ meets the adjustment amount $\Delta Power$ of a WF's output power, the power adjustment amount ΔP_i obtained by each controlled WT is optimal power distribution amount. During this process, it is also assessed whether a WT's UAC or DAC is zero (UAC is judged when a WF is increasing power, and DAC is judged when decreasing the power). WTs with UAC or DAC as zero will finish their cycle and record their current number of cycles n. The flow chart of the active power distribution algorithm is shown in Fig. 10 (the part within the green dashed box), and the calculation method of the adjustment amount $\Delta Power$ of a WF's output power is given in section 4. According to AGC command, when a WF's output power needs to be increased, the value of the transfer switch h in Fig. 10 is 1, and when the WF's output power needs to be reduced, the value of the transfer switch h is 2.

4. The dynamic interval control method (DICM)

The role of the active power control strategy of a WF is not only to quickly track AGC, but also to accurately control the output power of the WF within a certain range so that the deviation from the target value of AGC does not exceed the adjustment dead zone boundaries (ADZB). If it exceeds the ADZB, it will be subject to relevant assessment penalties. Since the output power of a WF fluctuates greatly, the closer it is to the ADZB, the easier it is to cross the line. In order to avoid assessment penalties, the output power is usually controlled within a certain range below the AGC curve. In fact, above the AGC curve, within the ADZB, as long as appropriate control is performed, there is still a lot of room for improvement in power generation efficiency. To maximize the power generation efficiency and accurately control the output power within an appropriate range, this paper proposes a DICM for a WF to establish the upper control interval limit (UCIL) and lower control interval limit (LCIL) of the dynamic control interval as the control set values, and adjust the set value of DICM in real time according to the rate of change of the output power of the WF, as shown in Fig. 9.

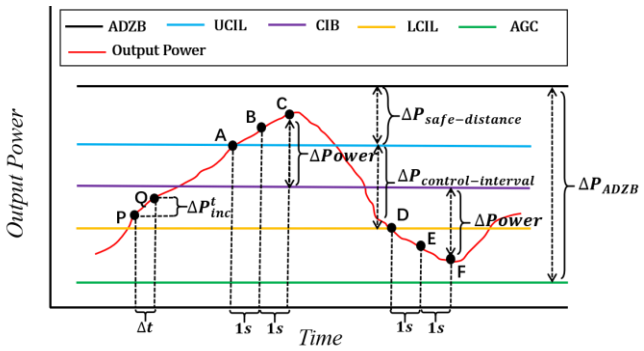

Fig. 9 *Principle of DICM*

The adjustment dead zone range ΔP_{ADZB} can be calculated from (22):

$$\Delta P_{ADZB} = P_{N-wf} D_{ad}\% \tag{22}$$

P_{N-wf} is the installed capacity of a WF, and $D_{ad}\%$ is the scaling coefficient for the adjustment dead zone range. Different countries and intervals have different regulations for the adjustment dead zone range, usually 1% -3% of the installed capacity of a WF. $\Delta P_{control-\text{interval}}$ is the dynamic control interval range, which determines the control accuracy of the output power of a WF.

The adjustment dead zone range ΔP_{ADZB} can be calculated from (22):

$$\Delta P_{ADZB} = P_{N-wf} D_{ad}\% \tag{22}$$

P_{N-wf} is the installed capacity of a WF, and $D_{ad}\%$ is the scaling coefficient for the adjustment dead zone range. Different countries and intervals have different regulations for the adjustment dead zone range, usually 1% -3% of the installed capacity of a WF. $\Delta P_{control-\text{interval}}$ is the dynamic control interval range, which determines the control accuracy of the output power of a WF. The smaller its value, the greater the difficulty of control. The greater the output power of a WF, the larger the fluctuation range. $\Delta P_{control-interval}$ can be calculated in (23) below:

$$\Delta P_{control-interval} = P_{output} D_{cr}\% \tag{23}$$

$D_{cr}\%$ is a control interval scale factor (CISF). When P_{output} runs beyond the UCIL to point A in Fig. 9, the adjustment condition for downward control is triggered, and the active power control system of a WF will send the power command to the controlled WTs. Due to the response lag of the output power of a WF (usually the response lag time is 1.5-2s), when P_{output} continues to increase to point C, the output power of the WF starts to decrease. As long as the output power at point C does not cross the ADZB, the assessment can be avoided and the output power reaches the maximum. Therefore, as long as the safety distance $\Delta P_{safe-distance}$ between the UCIL and the ADZB is updated in real time, the power generation efficiency of a WF can be maximized. This paper dynamically changes the value of $\Delta P_{safe-distance}$ according to the change rate of the output power of a WF, thereby adjusting the set value of the dynamic control interval in real time. When a WF operates to an arbitrary point P, and the increment of the output power P_{output} within a WT's response lag time is less than the safe distance $\Delta P_{safe-distance}$, i.e.,

$$\Delta P_{safe-distance} \geq S_{output-power} \Delta T_{lag} \tag{24}$$

The determined value of $\Delta P_{safe-distance}$ is the optimal value, where ΔT_{lag} is the response lag time of a WT, and $S_{output-power}$ is the changing rate of the output power of a WF, which can be calculated in (25) below:

$$S_{output-power} = \frac{\Delta P_{inc}^t}{\Delta T_{int}} \tag{25}$$

Here, ΔT_{int} is the interval of data collection, and ΔP_{inc}^t is the increment of P_{output} within ΔT_{int}, which can be calculated by the exponential weighted moving average algorithm:

$$\Delta P_{inc}^{t} = \frac{\sum_{i=0}^{N_t}(1-\alpha)^i \Delta P_{inc}^{i}}{\sum_{i=0}^{N_t}(1-\alpha)^i} \quad (26)$$

Where ΔP_{inc}^{i} is the increment of ΔP_{inc}^{i} within ΔT_{int} at the instant i before point P, N_t is the total number of calculation moments used by the exponentially weighted moving average algorithm, and α is the weighting coefficient, which can be calculated according to the (27):

$$\alpha = \frac{2}{N_t + 1} \quad (27)$$

The center line of the control interval is the control interval baseline (CIB). When P_{output} rises and crosses the UCIL, the difference $\Delta Power$ between the highest point C and the CIB of the dynamic control interval is the downward adjustment amount of the output power of a WF; When P_{output} drops below the LCIL, the adjustment condition for upward control is triggered. Due to a WT's response lag, the power starts to increase after reaching the lowest point F, the difference $\Delta Power$ between the point F and the CIB is the upward adjustment amount of the output power of a WF, and the value of $\Delta Power$ can be calculated by (28):

$$\Delta Power = S_{output-power}\Delta T_{lag} + 0.5\Delta P_{control-interval} \quad (28)$$

Where $S_{output-power}$ is the rate of change of P_{output} at the time when P_{output} passes out of the control interval (for example, points A and D in Fig. 9).

5. Active power dynamic interval control strategy of WF

For a WF responding to AGC, firstly, the control sequence of the controlled WTs is determined by selecting WTs with excellent DAP to participate in this power adjustment; Secondly, an active power distribution algorithm is designed to distribute the power adjustment amount of a WF to each controlled WT in a different way, and form a power command to send to the controlled WT; Then, an active power control strategy for a WF is designed, determining in real time whether the output power of the WF has been adjusted into the dynamic control interval and updating the output power adjustment amount of the WF in real time.

The proposed control strategy is written using Java script in MyEclipse development environment, as shown in Fig. 10. The control strategy consists of two independent modules: information flow (dashed arrows) and control flow (solid arrows). Information flow and control flow are two sets of independent runtime programs communicating with each other using the Modbus protocol. Information flow is responsible for collecting the basic operating states of WTs in real time, analysing WTs' DAP, and transmitting related information to links in the control flow.

1）Information flow

The information flow will first collect the operating states information $(v_i, \beta_i, \omega_i, P_i)$ of each WT at a sampling cycle of 250ms (ΔT_{IF}). The collected data are then used to calculate the DAP parameter values of each WT and the parameter value of $f_1^i(\beta)$. Following this, the total UAC and DAC of these controllable WTs at the current time are calculated in real time. The above calculated information will be transferred to the relevant control links in the control flow.

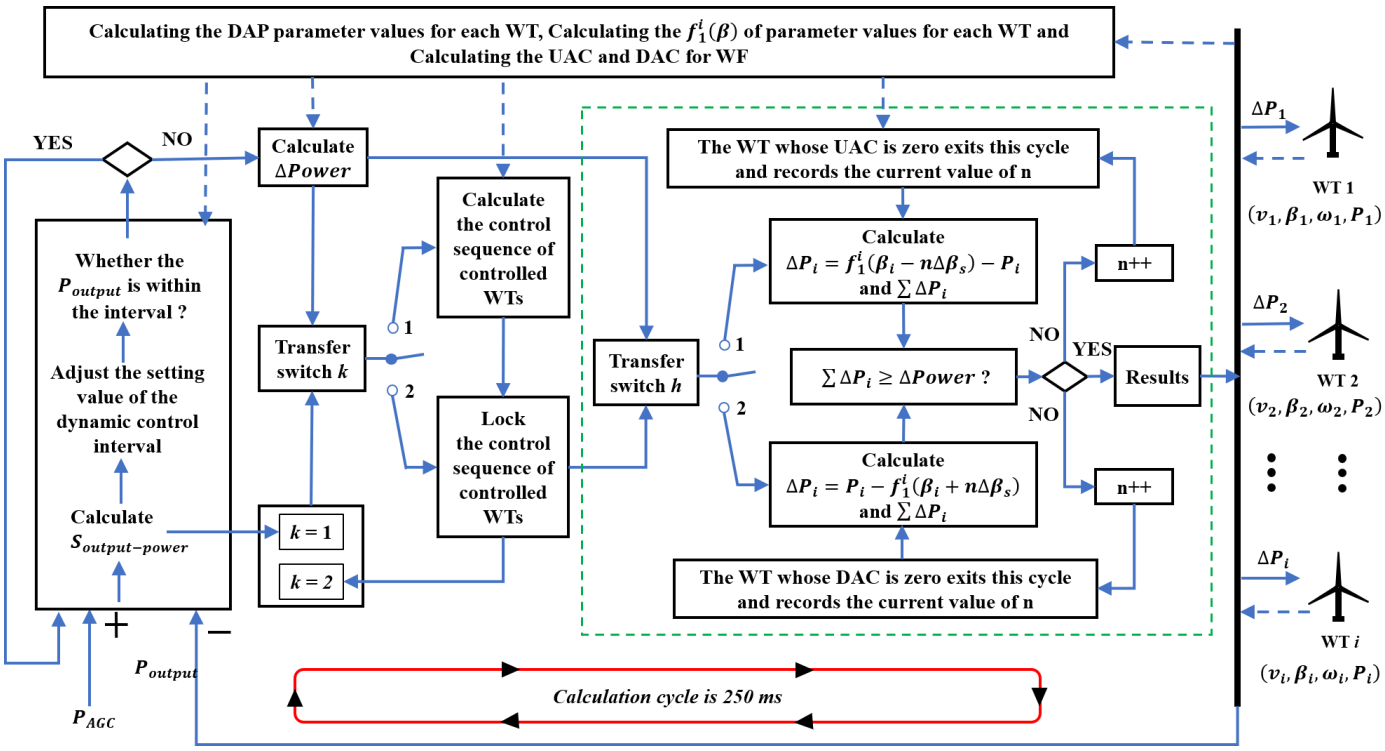

Fig. 10 *The algorithm process of active power dynamic interval control strategy for WF*

2）Control flow

The control flow is mainly composed of three steps: dynamic interval control, control sequence of controlled WTs and active power distribution The dynamic interval control calculates $S_{output-power}$ based on the output power P_{output} of a WF using (25) and adjusts its set value of UCIL, LCIL and CIB based on the value of the AGC command P_{AGC} and $S_{output-power}$ using (22)-(24). If P_{output} is in the control interval, it continues to read the information of P_{pref} and P_{output} for the next control cycle, meanwhile setting the value of the transfer switch k in Fig. 10 to 1. If P_{output} has exceeded the control interval, $\Delta Power$ will be calculated using (28) and transmitted to the control sequence of controlled WTs. Once $\Delta Power$ is received from the dynamic interval control, the optimal control sequence of control WTs is calculated based on the DAP parameter values of WTs. At the same time, the control sequence of controlled WTs will be locked, and the value of the transfer switch k in Fig. 10 set to 2. This status will be then transmitted to the active power distribution. Upon the receipt of the control sequence information, the active power distribution will calculate the adjustment amount output power that each controlled WT should undertake, combining WT's DAP parameter values, $f_1^i(\beta)$ and other information transmitted by the information flow. At this stage active power commands are formed and sent to each controlled WT.

Until now, a computation cycle of the information flow is completed. The computing time of the control flow ΔT_{CF} is about 250ms per cycle. In the next cycle, the dynamic interval control determines whether P_{output} is within the control interval. If it is still outside the control interval, $\Delta Power$ is re-calculated and transmitted to the locked control sequence of controlled WTs (at this time, the value of switch k is 2). Then the active power distribution updates the active power control command of the controlled WTs after receiving the new information. This control cycle will iterate until P_{output} returns to the control interval.

When P_{output} is outside the control interval, the control sequence of controlled WTs has to be locked in the first calculation cycle, otherwise WTs might be added to or removed out the controlled sequence in the next cycle calculation as the WTs' operating states information and DAP change in real time. If it is not locked, new added WTs will participate in power adjustment, while the old WTs are still executing the power command of the previous cycle. Due to the new WTs' participation in power adjustment, the output power of the WF will be over-adjusted.

6. The flowchart of the whole methodology

The flowchart of the whole methodology is shown in Fig. 11. It consists of three parts, namely offline data mining, information flow and control flow. The information flow uses the $f_1^i(\beta)$ and $g_1^i(\beta)$ parameters provided by offline data mining and the operating states information $(v_i, \beta_i, \omega_i, P_i)$ to calculate the evaluation index of WTs' DAP. The control flow uses these DAP information to calculate the control sequence of controlled WTs and each WT's ΔP_i.

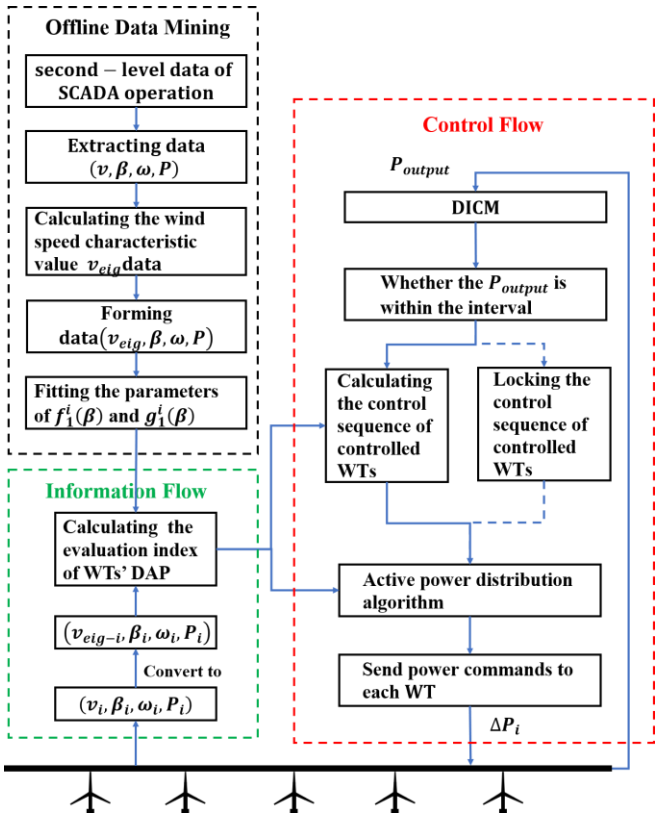

Fig. 11 *The flowchart of the whole methodology*

7. The verification of the proposed control strategy

The technologies and strategy developed in this paper have been implemented using Java script in MyEclipse. These include the extraction of effective wind speed characteristic features, the analysis of SCADA big data of WTs, the fitting of TCOSP, the calculation and analysis of DAP and the realization of active power dynamic interval control strategy. The control strategy is embedded in the independently developed energy management platform and successfully applied to many WFs in China. Initial real-world deployment has proved that the proposed control strategy improved regulation performance in AGC the power generation efficiency of WFs. The following present an example usage and its results of a practical application of a WF in the Northwest China Power Grid, which consists of 25 2MW doubly-fed induction generators. The relevant parameters of the WTs are shown in Table. S1 (see in Support Information).

In order to illustrate the effectiveness and feasibility of the proposed control strategy, a practical power adjustment process of the WF has been used for research and analysis. Before receiving the AGC command, the initial state information and DAP parameters of each WT in the WF are shown in Table. S3 (see in Support Information). Where, ΔP_{up}^i, ΔP_{down}^i, ΔP_{max}^i, $S_{power-up}^i$, $S_{power-down}^i$ are the UAC, DAC, MAC, UAR, DAR of the ith WT at the current moment. The No.2, No.17 and No.22 WTs are the template WTs and do not participate in the power regulation. The initial power of the WF is 37.07MW, and the target power of AGC is 31.07MW. The AGC assessment indexes of the regional power system [35] are shown in Table 1. In Table 1, t_{hx} is the lag time of the output power response of the WF, i.e. the time

from the WF receiving its AGC command to the time the output power changes reliably in the direction of AGC; $t_{0.9}$ is the response time of the output power of the WF, i.e. the time required for a WF to receive AGC commands until the output power adjustment amount reaches 90% of the difference between the AGC target power and the initial power; t_s is the output power adjustment time of the WF, i.e. the shortest time required for the WF to receive the AGC command until the output power stable. The setting values of each parameter of the control program are shown in Table. S4 (see in Support Information).

Table 1 AGC assessment indexes

Assessment indexes	t_{hx}	$t_{0.9}$	t_s
Satisfied condition	≤2s	≤12s	≤15s

7.1. The results of active power distribution

Given that the target power of AGC is 31.07MW, based on (28) and Table. S4, the output power adjustment amount $\Delta Power$ is calculated to be 5250kW. This can further be used to determine the control sequence of control WTs by (20). The calculation results show that all WTs except for the template WTs participate in this power adjustment. The output power adjustment of each WT ΔP_i is presented and also compared with the calculation results of proportional distribution algorithm (PDA), ability weight distribution algorithm (AWDA), multi-objective optimization algorithm (MOOPA), as shown in Table. S5 (see in Support Information). ΔP_i^{PDA}, ΔP_i^{AWDA}, ΔP_i^{MOOPA} and ΔP_i^{paper} in the Table. S5 are the results of PDA, AWDA, MOOPA and the method in this paper. $P_{pro}\%$ represents the proportion of the output power of each controlled WT to the total output power of all controlled WTs (the output power of the WF minus the output power of all template WTs):

$$P_{pro}\% = \frac{P_i}{P_{output} - P_2 - P_{17} - P_{22}} \times 100\% \quad (29)$$

7.2. The adjustment synchronization of controlled WTs before and after application

Fig. 12 shows the output power curve of the WF where the horizontal coordinate zero denotes the moment when all controlled WTs receive the power command. The response lag time t_{hx} of the output power is 1.6s, the response time $t_{0.9}$ is 3.75s, and the adjustment time t_s is 4.8s, all of which are far superior to the AGC assessment indexes requirements. Fig. 13 - Fig. 15 shows the output power curve of each controlled WT (shown in groups according to the output power). Although each WT undertakes different power adjustments, they reach their respective target powers almost simultaneously. It can be seen that the output power change between each WT are synchronized, and the output power change between the single WT and the entire WF are synchronized.

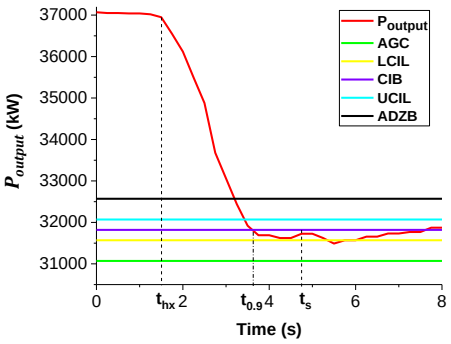

Fig. 12 *The output power curve of the WF after the application*

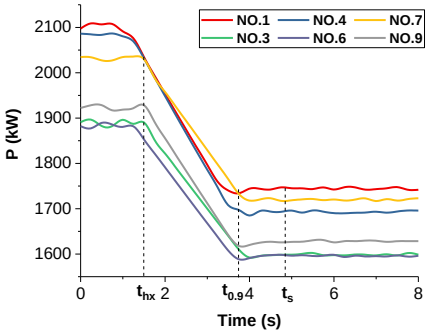

Fig. 13 *The change curve of WTs with high output power after the application*

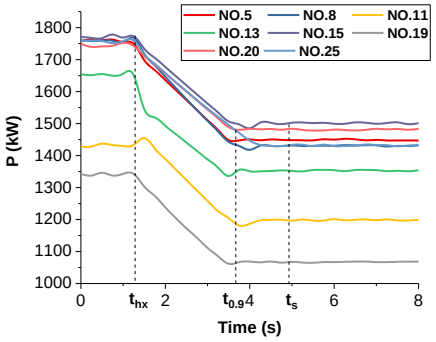

Fig. 14 *The change curve of WTs with medium output power after the application*

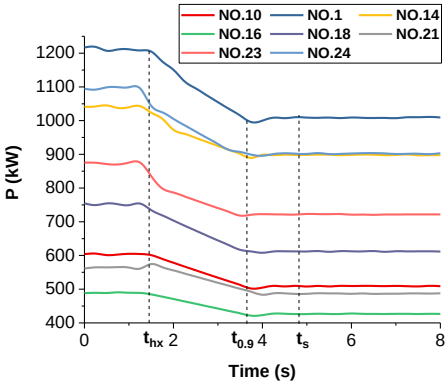

Fig. 15 *The change curve of WTs with low output power after the application*

The mean values E_{thx} , $E_{t0.9}$, E_{ts} and standard deviations σ_{thx}, $\sigma_{t0.9}$, σ_{ts} of t_{hx}^i, $t_{0.9}^i$and t_s^i for all controlled

WTs are calculated, and presented in Table 2. It can be seen from Table 2 that E_{thx}, $E_{t0.9}$, and E_{ts} are all very close to 1.5s, 3.75s and 4.8s, respectively, andσ_{thx}, $\sigma_{t0.9}$, and σ_{ts} are all less than 0.01, indicating that t_{hx}^i, $t_{0.9}^i$and t_s^i of each WT are mainly distributed near their mean values. Table. S6 shows the adjustment amount $\Delta\beta_i$ of the pitch angle of each controlled WT at the time of 3.75s, and Table 3 shows the average and standard deviation of $\Delta\beta_i$. According to Table. S6 and 3, the adjustment amount of the pitch angle of each controlled WT are very close to around 2.40.

Table 2 Mean and standard deviation of the corresponding indicators of the dap of the controlled WTs after the application

	Mean			Standard deviation		
	E_{thx}	$E_{t0.9}$	E_{ts}	σ_{thx}	$\sigma_{t0.9}$	σ_{ts}
Results	1.62	3.7	4.9	0.092	0.081	0.096

Table 3 The average and standard deviation of $\Delta\beta_i$

	Mean	Standard deviation
Results	2.40	0.0598

Before application, the active power control method of the WF used PI+ AWDA. Fig. 16 and 17 show the control results of a power adjustment process of the WF before the application. Fig. 16 shows the WF's output power change curve. Fig. 17 shows the controlled WTs' output power change curve. Table 4 shows the response time of the WF and each controlled WT.

Table 4 the response time of the WF and each controlled WT before the application

	WF	The controlled WTs				
		NO. 13,20	NO. 8,11	NO. 10	NO. 15	NO. 1,3,4
	$t_{0.9}$	$t_{0.9}^{13,20}$	$t_{0.9}^{8,11}$	$t_{0.9}^{10}$	$t_{0.9}^{15}$	$t_{0.9}^{1,3,4}$
The response time/s	10	5.2	8.1	8.6	9.2	10.1

The response time $t_{0.9}^i$ of each controlled WT varies greatly. Among them, the max value $max\{t_{0.9}^i\}$ of $t_{0.9}^i$ are $t_{0.9}^1$, $t_{0.9}^3$, and $t_{0.9}^4$, with a value of 10.1s, and the min value $min\{t_{0.9}^i\}$ of $t_{0.9}^i$ are $t_{0.9}^{13}$ and $t_{0.9}^{20}$, with a value of 5.2s. The WF's response time $t_{0.9}$ is 10s, which is very close to $max\{t_{0.9}^i\}$. This illustrates that the WF's $t_{0.9}$ depends on $max\{t_{0.9}^i\}$. Before the application, the power adjustment between the controlled WTs was not synchronized, which affected the rapidity of the output power adjustment of the whole WF.

These results prove that, with the proposed control strategy, not only the output power response time of each controlled WT is consistent with the corresponding response time of the WF, but also the adjustment amount of the pitch angle of each controlled WT are very similar. The power adjustment synchronization between each WT and between WTs and the WF are achieved, and the balance of the adjustment amount of the pitch angle is optimized.

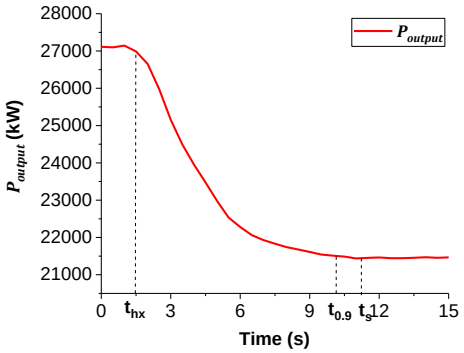

Fig. 16 *The WF's output power change curve before the application*

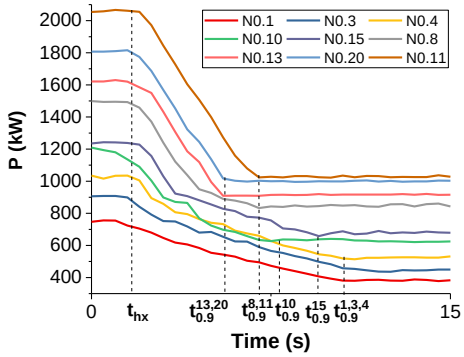

Fig. 17 *the controlled WTs' output power change curve before the application*

If a WF is composed of multiple types of WTs which apply various pitch angle control methods, their pitch rates will be different. When calculating the active power adjustment amount ΔP_i undertaken by a WT, it is necessary to convert the UAR, DAR, $f_1^i(\beta)$ and abscissa in Fig. 8 to the time coordinate. In the time coordinate, ΔP_i is calculated based on the principle of consistent power adjustment time.

7.3. The responsiveness of the WF to AGC

When the control sequence of controlled WTs and the output power adjustment amount $\Delta Power$ of a WF are determined, the value of $t_{0.9}$ of WF's output power depends on $E_{t0.9}$ and $\sigma_{t0.9}$. For a same controlled WT, the $t_{0.9}^i$ depends on the output power adjustment amount ΔP_i. The larger ΔP_i is, the larger $t_{0.9}^i$ is, and vice versa. However, $\sum \Delta P_i$ is fixed because $\Delta Power$ has been determined. Therefore, the smaller the difference of $t_{0.9}^i$ of the controlled WTs, the more concentrated they are around the mean value, i.e. the smaller the value of $\sigma_{t0.9}$, the value of $t_{0.9}$ of a WF's output power is smaller. Under the PDA, AWDA, MOOPA, $t_{0.9}^i$ of any controlled WT can be approximately calculated by (30):

$$\left[t_{0.9}^i\right]_A \approx \frac{\Delta P_i^A}{S_{power-down}^i S_{\Delta\beta}} + t_{hx} \qquad (30)$$

Where, A stands for PDA, AWDA, MOOPA, $S_{\Delta\beta}$ is the pitch angle adjustment rate, which is constant. In normal operation, a WT's $S_{\Delta\beta}$ is usually 1-2deg/s during power regulation. In

this case study, the $S_{\Delta\beta}$ for each WT is 1.2deg/s. Then, the comparison of the mean value and standard deviation under the PDA, AWDA, MOOPA and this paper are as show in Table 5. Among the four values of $E_{t0.9}$ and $\sigma_{t0.9}$, the result under the proposed control strategy is the smallest, especially in $\sigma_{t0.9}$, the control result in this work is far less than the other three.

Therefore, under the proposed control strategy, the rapidity of WF in responding to AGC is better than PDA, AWDA and MOOPA.

Table 5 The comparison of the mean value and standard deviation

	$E_{t0.9}$	$\sigma_{t0.9}$
PDA	3.73	0.42
PWDA	3.91	0.68
MOOPA	4.02	1.13
This paper	3.70	0.081

7.4. The accuracy of the output power of the WF

Fig. 18 shows the output power curve of the WF after $t_{0.9}$, which is close to the ADZB, and it does not cross the ADZB. In the period of 7-9.5s, the output power continues to rise, triggering the adjustment condition of dynamic control interval. The setting value of dynamic control interval is adjusted downward, and the output power is adjusted to the new control range as well; In the period of 20.5-23.5s, the output power is relatively stable, and the setting value of the dynamic control interval is adjusted upward.

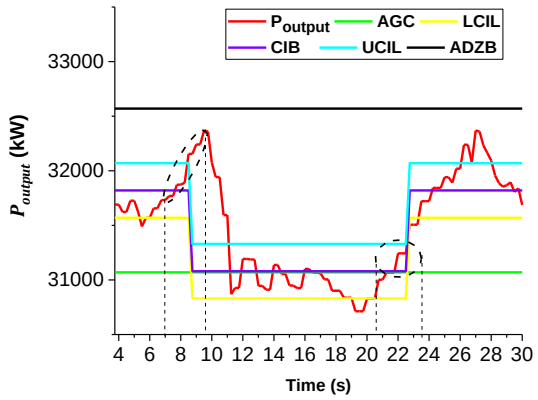

Fig. 18 *The output power curve of the WF after* $\boldsymbol{t_{0.9}}$

Fig. 18 also indicates that when the output power exceeds the LCIL or UCIL, the adjustment condition for output power upward control or downward control will be triggered. The output power is always controlled within the range of $\pm 0.5D_{cr}\%$ with the CIB as the center line. Hence, the DICM dynamically adjusts the setting value of the control interval according to the real-time change rate of the output power of the WF to ensure that the output power does not exceed the ADZB and be as close as possible to the ADZB to maximize the efficiency of power generation. At the same time, when the output power exceeds the control interval, DICM can make it quickly return to set interval to ensure the stable output of wind power.

In order to further illustrate that the proposed control strategy can improve the accuracy of the output power of a WF and reduce frequent adjustment of WTs, the fixed interval control method (FICM) and non-interval control method (N-ICM) are replaced with the DICM, meanwhile the relevant data are recorded. The control results and the comparison, as shown in Fig. 19.

Fig. 19 (a) shows the results of control using the FICM. During the period of 21s-25s, the output power continues to rise. The FICM cannot timely adjust the set value of the control interval and the distance between the output power and the ADZB based on the real-time change of the output power of the WF, which makes it easier for the output power to exceed the ADZB, causing unnecessary assessment penalty losses. Fig. 19 (b) shows the results of the N-ICM. The essential difference from the DICM is that there is no upper and lower bound near the WF's output power target value. When the output power is adjusted near the target value, the output power of the WF fluctuates greatly. In order to track the target value in real time, the output power frequently oscillates near the target value, reducing the accuracy of the output power, and bringing frequent adjustment of WTs' power, eventually will increase the mechanical losses. Fig. 19 (c) and Fig. 19 (d) illustrate the results of using DICM, where Fig. 19 (c) is the scenario with a CISF value of 3% and Fig. 19 (d) is the scenario with a CISF value of 2%. As the value of CISF is reduced, the number of times that the output power curve in Fig. 19 (d) exceeds the UCIL or LCIL is more than that in Fig. 19 (c), i.e. the number of output power adjustment is increased. It can be seen that if the value of CISF is set too large, although the number of output power adjustment can be reduced, the control accuracy is also reduced; if the value of CISF is set too small, even though the control accuracy can be improved, but the number of output power adjustment is also increased at the same time. Hence, the determination of CISF is crucial. In this paper, CISF is set to a fixed value. How to adjust the CISF value scientifically and reasonably according to the real-time fluctuation of output power of a WF and the DAP of the controlled WTs is the content of the author's subsequent research.

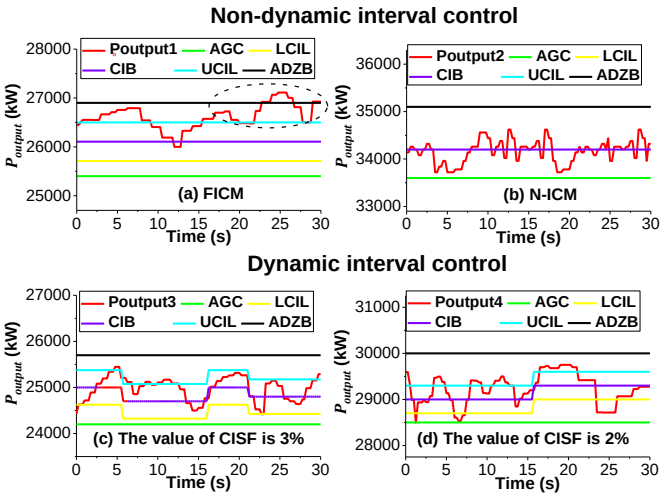

Fig. 19 *Comparison of control results between DICM, FICM and N-ICM*

7.5. *The efficiency of power generation before and after application*

In order to further illustrate that the control strategy can not only improve the rapidity, accuracy of a WF responding to AGC, but also maximize its efficiency of power generation, the actual control results before and after the application of the control strategy are compared and analysed in Fig. 20. As the output power of the WF fluctuates significantly, the closer it is to the ADZB, the easier it is to cross the line. Without the application of the control strategy, the output power is controlled within a certain range below the AGC curve, as shown in the Fig. 20 (a) and Fig. 20 (b). Once the proposed control strategy is applied, the output power is controlled more smoothly between the AGC curve and the ADZB. Most importantly it does not cause the output power exceeding the ADZB, thus avoiding re-assessment, and improving the power generation efficiency, as shown in the Fig. 20 (c) and Fig. 20 (d). The power generation beyond the AGC curve is regarded as the increased power generation. During the statistical period (120s) of the curves c and d in Fig. 20, the power generation efficiency is increased by 2.59% and 3.02%, as shown in Table 6.

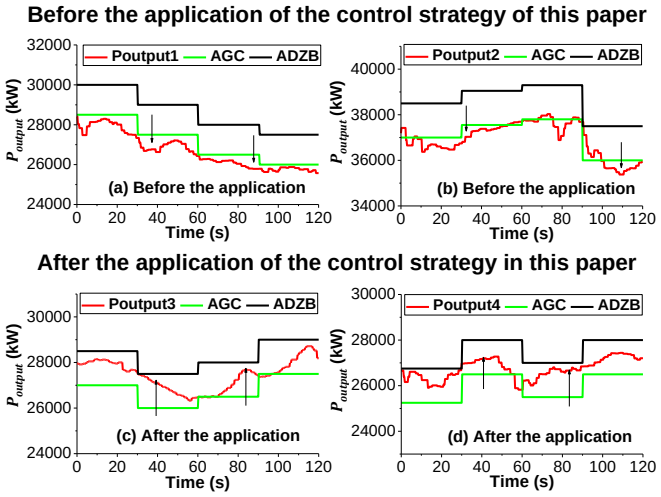

Fig. 20 *The actual control results before and after the application of the control strategy in this paper*

Table 6 Improvement of power generation efficiency in the statistical period

Statistical period	Increased power generation （kWh）	Increased power generation ratio （%）
Statistical period of curve c(120s)	24.1	2.59%
Statistical period of curve d(120s)	27.2	3.02%

The WF in the case study is located on the plains of the plateau in Northwest China. The main wind directions throughout the year are southeast and northwest. In the main wind direction, it is relatively weakly affected by the wake effect. In the direction of non-mainstream winds, the influence of wake effect is relatively obvious. Active power control strategies for WFs considering wake effect are under study.

8. Conclusion

The TCOSP mining method extracting the complex relationship from the output data, input data and control data reveals the internal relations between WTs' DAP and their operating states. The proposed control strategy has fully coordinated the DAP of WTs with different operating states, as such, it achieves the goal to match the active power distribution control with the DAP of WTs. The control strategy is tested and evaluated using the real operation data from a WF of Northwest China. Initial experiment results show that the proposed strategy improves the timeliness and accuracy of the WF responding to AGC, and the results also prove the effectiveness and validity of the developed methods.

This developed method is derived from actual data, without any simplified assumptions for WTs and modifying the central control program of the single WT, which can improve the control accuracy and facilitate practical application. In future research, the DAP of WFs will be studied to achieve synchronization of power adjustment between WFs and improve the rapidity of WF groups with the response to AGC.

9. Acknowledgments

The authors give their sincere appreciations to the support of National Natural Science Foundation of China (No. U1810126), Qinghai Key R & D and transformation projects (No. 2019-GX-C27), Qinghai Enterprise Research T & I Special projects (No. 2020-GX-C15).

Case study auxiliary explanation, auxiliary data for TCOSP analysis and auxiliary data for proposed control strategy verification are noted in supporting information.

10. References

[1] Global Wind Energy Council. Global Wind Statistics 2019; May. 2020.

[2] Hasanien, H. and El-Fergany, A.: 'Symbiotic organisms search algorithm for automatic generation control of interconnected power systems including wind farms', IET Generation, Transmission & Distribution, 2017, 11, (7), pp. 1692-1700

[3] Wei, S., Zhou, Y., Xu, G.: 'Motor-generator pair: a novel solution to provide inertia and damping for power system with high penetration of renewable energy', IET Generation, Transmission & Distribution, 2017, 11, (7), pp. 1839-1847

[4] Ouyang, J., Li, M., Diao, Y.: 'Active control method of large-scale wind integrated power system with enhanced reactive power support for wind speed fluctuation', IET Generation, Transmission & Distribution, 2018, 12 (21), pp. 5664-5671

[5] Ahmad, K., Mohammad, N. and Quamruzzaman, M.: 'Review on Frequency Adjustment for Power Systems with Grid Connected Wind Farm', 2019 International Conference on Robotics, Electrical and Signal Processing Techniques (ICREST), Dhaka, Bangladesh, 2019, pp. 617-621.

[6] Aziz, A., Than, A., and Stojcevski, A.: 'Frequency regulation capabilities in wind power plant', Sustainable Energy Technologies & Assessments, 2018, 26, pp. 47-76

[7] Zhang, S., Mishra, Y., Shahidehpour, M.: 'Fuzzy-Logic Based Frequency Controller for Wind Farms Augmented With Energy Storage Systems', IEEE Transactions on Power Systems, 2016, 31, (2), pp. 1595-1603

[8] Liu, J., Wen, J., Yao, W., et al.: 'solution to short-term frequency response of wind farms by using energy storage systems', IET Renewable Power Generation, 2016, 10, (5), pp. 669-678

[9] Liu, Y., Du, W., Xiao, L., et al.: 'sizing Energy Storage Based on a Life-Cycle Saving Dispatch Strategy to Support Frequency Stability

of an Isolated System With Wind Farms', IEEE Access, 2019, 7, pp. 166329-166336
[10] Huang, S., Wu, Q., Guo, Y., et al.: 'Optimal active power control based on MPC for DFIG-based wind farm equipped with distributed energy storage systems', International Journal of Electrical Power & Energy Systems, 2019, 113, (DEC.), pp. 154-163
[11] Mosaad, M., Alenany, A., and Abu-Siada, A.: 'Enhancing the performance of wind energy conversion systems using unified power flow controller', IET Generation, Transmission & Distribution, 2020, 14, (10), pp. 1922-1929
[12] Khamaira, M., Abu-Siada, A., Islam, S.: 'Application of high temperature superconductor to improve the dynamic performance of WECS', 2015 IEEE Power & Energy Society General Meeting, Denver, Denver, CO, 2015, pp. 1-6
[13] Dozein, G., Monsef, H., and Wu, B.: 'An Optimal Frequency Control Method Through a Dynamic Load Frequency Control (LFC) Model Incorporating Wind Farm', IEEE Systems Journal, 2018, 12, (1), pp. 392-401
[14] Zhao, X., Yan, Z., Xue, Y., et al.: 'Wind Power Smoothing by Controlling the Inertial Energy of Turbines With Optimized Energy Yield', IEEE Access, 5, pp. 23374-23382
[15] Prasad, R., and Padhy, N.: 'Synergistic Frequency Regulation Control Mechanism for DFIG Wind Turbines With Optimal Pitch Dynamics', IEEE Transactions on Power Systems, 2020, 35, (4), pp. 3181-3191
[16] Zhao, H., Wu, Q., Guo, Q., et al.: 'Distributed Model Predictive Control of a Wind Farm for Optimal Active Power ControlPart II: Implementation With Clustering-Based Piece-Wise Affine Wind Turbine Model', IEEE Transactions on Sustainable Energy, 2015, 6, (3), pp. 840-849
[17] Chen, Z., Wang, H., Jiang, Q.: 'Optimal control method for wind farm to support temporary primary frequency control with minimised wind energy cost', IET Renewable Power Generation, 2015, 9, (4), pp. 350-359
[18] Siniscalchiminna, S., Ocampomartinez, C., Bianchi, F., et al.: 'Partitioning approach for large wind farms: Active power control for optimizing power reserve', 2018 IEEE Conference on Decision and Control (CDC), Miami Beach, FL, 2018, pp. 3183-3188.
[19] Siniscalchi-Minna, S., Bianchi, F., Ocampo-Martinez, C.: 'Predictive control of wind farms based on lexicographic minimizers for power reserve maximization'. 2018 Annual American Control Conference (ACC), Milwaukee, WI, 2018, pp. 701-706.
[20] Bubshait, A., Alsaleem, A., Simões, M. 'Centralized Power Reserve Algorithm of De-loaded Wind Farm for Primary Frequency Regulation', 2018 IEEE Energy Conversion Congress and Exposition (ECCE), Portland, OR, 2018, pp. 423-429.
[21] Siniscalchiminna, S., Bianchi, F., Depradagil, M., et al.: 'A wind farm control strategy for power reserve maximization', Renewable energy, 2019, 131, pp. 37-44.
[22] Ma, S., Geng, H., Yang, G., et al.: 'Clustering-Based Coordinated Control of Large-Scale Wind Farm for Power System Frequency Support', IEEE Transactions on Sustainable Energy, 2018, 9, (4), pp. 1555-1564
[23] Guo, Y., Kabamba, P., Meerkov, S., et al.: 'Quasilinear Control of Wind Farm Power Output', IEEE Transactions on Control Systems and Technology, 2015, 23, (4), pp. 1555-1562
[24] Badihi, H., Zhang, Y., Hong, H., et al.: 'Active power control design for supporting grid frequency regulation in wind farms', Annual Reviews in Control, 2015, 40, (SEP.), pp. 70-81
[25] Chen, Z., Liu, J., Lin, Z., et al.: 'Closed-loop active power control of wind farm based on frequency domain analysis', Electric Power Systems Research, 2019, 170, (MAY), pp.13-24
[26] Zhang, W., Fang, K.: 'Controlling active power of wind farms to participate in load frequency control of power systems', IET Generation Transmission & Distribution, 2017, 11, (9), pp. 2194-2203
[27] Zhang, X, Chen, Y., Wang, Y., et al.: 'Deloading Power Coordinated Distribution Method for Frequency Regulation by Wind Farms Considering Wind Speed Differences', IEEE Access, 2019, 7, pp. 122573-122582
[28] Liu, J., Zhang, B., Zhao, T.: 'Research on Wind Farm Active Power Dispatching Algorithm Based on Fuzzy Evaluation', Transactions of China Electrotechnical Society, 2019, 34(04), pp.786-794
[29] Latif, A., Das, D., and Barik, A.: 'Comparative performance evaluation of WCA-optimised non-integer controller employed with WPG–DSPG–PHEV based isolated two-area interconnected microgrid system', IET Renewable Power Generation, 2019, 13, (5), pp. 725-736
[30] Latif, A., Das, D., Barik, et al.: 'Illustration of demand response supported co-ordinated system performance evaluation of YSGA optimized dual stage PIFOD-(1+PI) controller employed with wind-tidal-biodiesel based independent two-area interconnected microgrid system', IET Renewable Power Generation, 2019, 14, (6), pp. 1074-1086
[31] Teow, M., Chiu, H., and Tan, R.: 'A computational modelling of wind turbine mechanical power and its improve factor determination', 2016 IET Clean Energy and Technology Conference, Kuala Lumpur, 2016, pp. 1-8
[32] Tang, X., Yin, M., Shen, C., et al.: 'Active Power Control of Wind Turbine Generators via Coordinated Rotor Speed and Pitch Angle Regulation', IEEE Transactions on Sustainable Energy, 20, (2), pp. 822-832
[33] Dong, Z., Li, Z., Dong, Y., et al.: 'Fully-Distributed Deloading Operation of DFIG-based Wind Farm for Load Sharing', IEEE Transactions on Sustainable Energy, doi: 10.1109/TSTE.2020.3002690.
[34] Liu, Y., Wang, L., Meng, E., et al.: 'Dynamic Adjustment Performance of Wind Turbines Based on Measured Data', Power System Technology (in China), 2020, https://doi.org/10.13335/j.1000-3673.pst.2020.0253
[35] Sun, X., Liu, X., Cheng, L., et al.: 'Parameter Setting of Rapid Frequency Response of Renewable Energy Sources in Northwest Power Grid Based on Coordinated Control of Multi-frequency Regulation Resources', Power System Technology (in China), 2019, 43, (5), pp. 1760-1765